Supplemental Material

Journal of Physical Oceanography DOI:10.1175/JPO-D-19-0128.1

Interior Water-Mass Variability in the Southern Hemisphere Oceans during the Last Decade

Esther Portela, Nicolas Kolodziejczyk, Christophe Maes, and Virginie Thierry

Univ. Brest, Laboratoire d'Océanographie Physique et Spatiale, CNRS, IRD, Ifremer, Plouzané, France

Corresponding author: Esther Portela, eportelah@gmail.com

Supplementary Material

1.Uncertainty computation and MLD smoothing

Data-based studies, mainly those with gridded fields, contain several sources of uncertainty: sampling and interpolation error and uncertainties due to the residual of estimations are among the most common ones. The error derived from sampling bias is difficult to estimate, however, the map of percentage of variance (Figure 2) works as a good proxy of this error, showing the latitudinal gradient in the data availability. The uncertainty associated to the volume trend computation is given by the significance level. In our discussion we only took in account the σ-τ classes with trends significant at 95%, which are represented by the dots in Figure 4b, c and d.

After performing several preliminary tests, we have confirmed that uncertainty in the subduction rate is the most important source of error among all the computations performed in this study. Moreover, of the three components of subduction, it is the lateral induction due to the horizontal gradient of the MLD which accounts for most of the error. We verified, by computing the MLD with different criteria, that the detection method of the MLD used in this study was the more accurate for our data set and region. Afterwards, we identified the two processes that are introducing the main variability to the MLD computation: the MLD interpolation and the smoothing.

To account for the MLD variability due to the interpolation process, we computed the mapping error as the standard deviation between three different interpolation methods as done in Pellichero et al. (2018): from the previously computed MLD of each single profile we carried out objective mapping following (i) the method of Kirill Pankratov, (http://globec.whoi.edu/software/saga/objmap.m) and (ii) objective analysis based on Barnes technique (Barnes 1964). In addition (iii) we obtained the MLD from previously gridded fields of temperature and salinity obtained from ISAS. The error in MLD mapping was then propagated to the total subduction computation and the resulting error bars are shown in Figure 4a of the main manuscript.

The second important source of variability of the subduction is the smoothing of the MLD. Different methods as Gaussian filter and convolution were tested in this study. The choice of the running mean was based on the best compromise between reliability and physical meaning that this method provided. While the results obtained by different methods were somehow comparable, one of the key factors to chose the running mean was that the other possibilities propagated the blank area given by the land mask (NaN in the MATLAB language), what lead to an important loss of information.

In order to set the adequate moving window of the running mean, we performed several tests. The lateral induction (the term of subduction which is the most sensitive to the MLD gradient) was computed using ISAS and ECCOv4 without and with only MLD smoothing with different moving windows for the running-mean. The result is shown in Figure S1.

As expected, and in contrast with ISAS, the main lateral induction structures and magnitude from ECCOv4 does not show an important change with or without MLD smoothing. ISAS MLD has to be considerably smoothed in order to remove all the fine-scale structures. These structures comprise the unresolved scales (by the Argo network) and the lack of consistency in ISAS between the MLD gradient and the velocity field. On the contrary, in ECCOv4, the MLD gradient is consistent with the velocity field, and only a short moving window is needed to remove the small-scale features observed around the Drake Passage and other specific locations, mainly at the southern border of the domain.

Figure S1 suggests that the magnitude and dominant structures of the induction as computed from ECCOv4 can be a reference to validate the moving window chosen for the running mean applied on the MLD from ISAS. Panel c) shows similar structures as those found in ECCO (panels e and f) while shorter moving windows in ISAS result in a too noisy induction also characterized by too high magnitude.

It is worth noticing that in both of the modeling studies of Langlais et al. (2017) and Downes et al. (2017) subduction appears to be a patchy field due to chaotic behaviors of the ACC and stationary Rossby waves. With the Argo dataset, the resolution (3°x3°) is not enough to resolve these small-scale structures and therefore in this study we focus only in the medium-large scale processes.

The effect of the moving-window size on the resulting subduction magnitude from ISAS along a zonal section at 40°S, can be seen in Figure S2. As observed, the subduction magnitude converges to an asymptotic value, this suggests that after this value, a greater moving window is not necessary linked to a smoother field. Given this results, and the comparison between ECCOv4 and ISAS showed in Figure S1, the moving window of the running mean for the MLD was set to 10º.

Smoothing is a very common procedure when working with data, however it is rarely reported in detail in the literature. Also, smoothing is subjective, as it is not possible to quantify the suitability of a specific method over all the possible ones, rather, the criterion is often chosen as a trade off between the preservation of the main characteristics of the given field and the possibility to obtain reliable, robust and physically consistent conclusions.

Here we have learned that the degree of smoothing, even if it does not change significantly the spatial patterns of the subduction terms, has a pivotal effect in their magnitude and therefore it is indispensable to carefully describe it. In addition, it has been shown how in the case of this study, this smoothing is necessary to find physically consistent patterns, otherwise undetectable.

Finally, the uncertainty in transformation is mainly correlated to that of subduction. The remaining source of error in the transformation computation is given by the residual of the linear regression from the linear equations system which is indicated in the text to be of the order 10^{-11} with maximum at 10^{-5}.

2. Comparison ISAS vs ECCOv4: Lateral Induction computation

As previously stated, subduction is a critical computation with a high uncertainty. Since transformation relies on volume trend and subduction, it is important to ensure the robustness of our results regarding the subduction field. To this end, in addition to the Figure S1, which shows important aspects of the smoothing process, we have computed induction with ECCOv4 following two different methods: (I) by obtaining the induction field for every single month over the period 2006-2015 and time-averaging the final induction (fine temporal resolution). (ii) Following the same procedure as with ISAS, that is, computing induction for every climatological month and then time-averaging the final induction (coarse temporal resolution). The deepest MLD over the entire period was chosen in both cases. The resulting induction fields together with the lateral induction computed from ISAS climatological monthly fields are shown in Figure S3. In all the cases we used the same smoothing scale (10º of moving window).

Despite the differences between the subduction from ISAS (panel a) and ECCOv4 (panel b and c), the main patterns of subduction/obduction persist in both cases. When computed with ECCOv4, the two induction fields (panel b and c) show very similar structures and magnitude; the finely-resolved induction (panel c) presents slightly more spatial variability than the climatologically computed induction (panel b).

Of particular interest are the dipolar, or rather, multi-polar structures, between the East of Australia and New Zealand, and in the central South Pacific. These regions of strong subduction/obduction are present in all three panels of Figure S3 which increases the confidence in our computations. Their location coincides with the narrowing of the main ACC flow (blue lines) and its fronts (black lines) which suggests that it could be a topographically-induced feature due to the standing meanders of the ACC rather than MLD-gradient derived. In fact, these dipolar structures are somehow compensated by the MLD gradient. When computed with ECCOv4, the lateral induction obtained without smoothing shows a much weaker dipoles (Figure S1d). The dipoles become more evident with the increase of the MLD smoothing level (Figure S1e, f), while the velocity field is always the same.

3. Components of the transformation term:

Figure S4 shows a more detailed view of the relative contribution of the isopycnal and diapycnal transformation components, as well as the exchange flow in σ-τ coordinates. We can see that isopycnal transformation dominates over all the AAIW density layers (highlighted with red squares) while diapycnal transformations are key for the total formation within the SAMW range (marked with black squares). The exchange flow becomes important for the spicier varieties of the SAMW and for the less spice IW.

Figures:

Figure S1

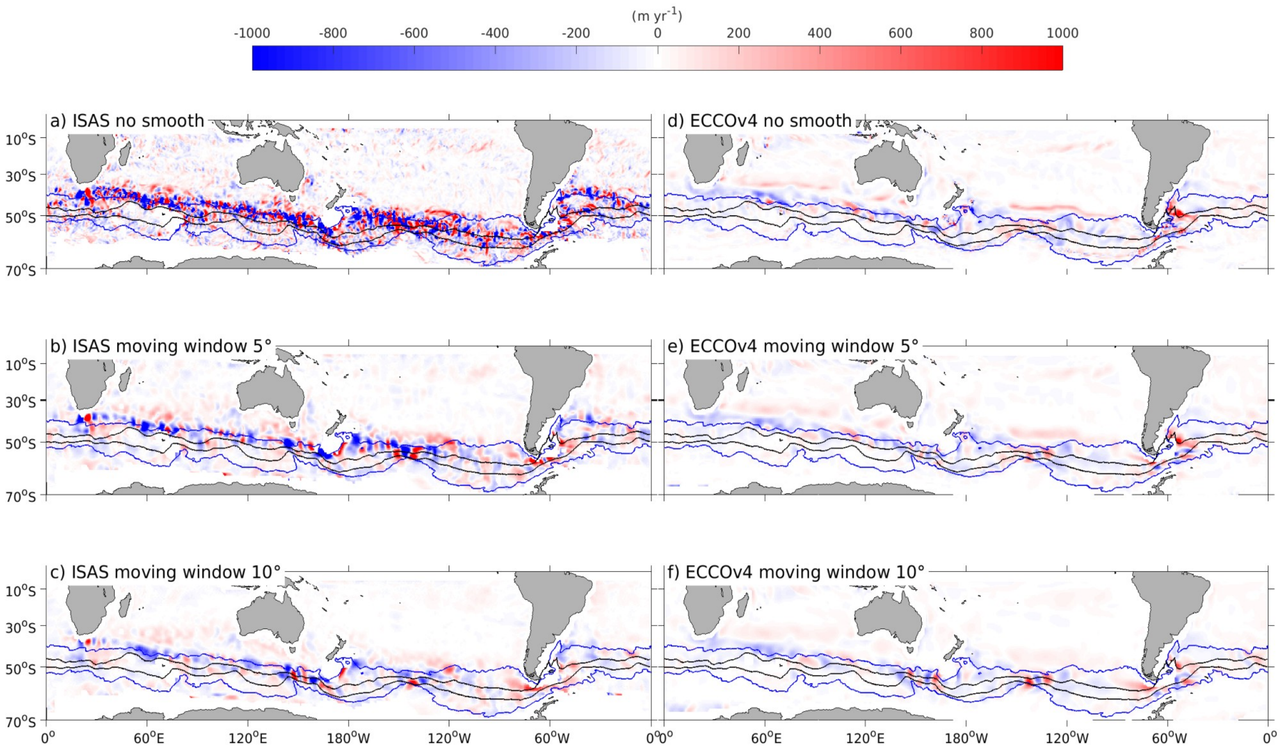

Figure S1. Lateral induction computed from (a-c) ISAS and (d-f) EECOv4 by time-averaging the monthly climatological data. Different smoothing was applied in each row. A,d) No smooth was applied to the MLD field. (b,e) the running mean smoothing method with a moving window of 5º was applied to the MLD. (c,f) the running mean smoothing method with a moving window of 10º was applied to the MLD. In all the panels blue contours represent the northern and southern boundaries of the ACC computed as the outermost close contours of sea surface height through the Drake passage. The black lines inside are the Subantarctic and Polar fronts from North to South respectively as computed by (Sallée et al. 2008).

Figure S2

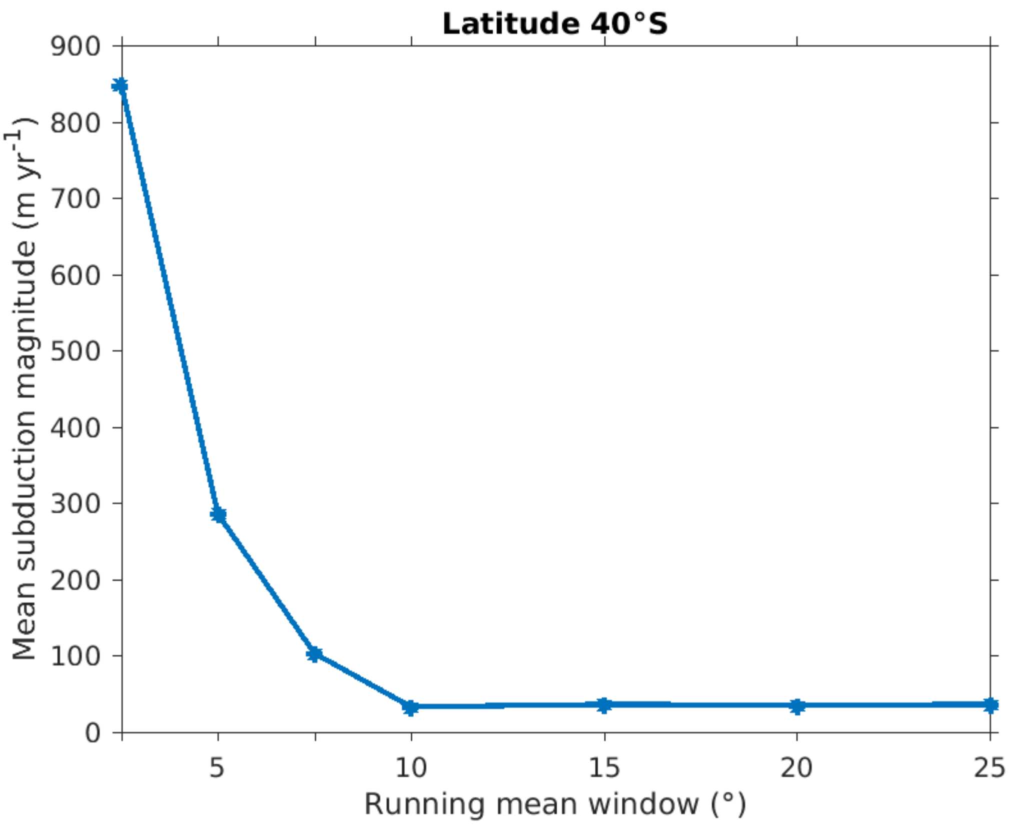

Figure S2. Average relation between the degree of the smoothing (given by the window of the running mean) and the magnitude of subduction along a zonal section at 40°S

Figure S3

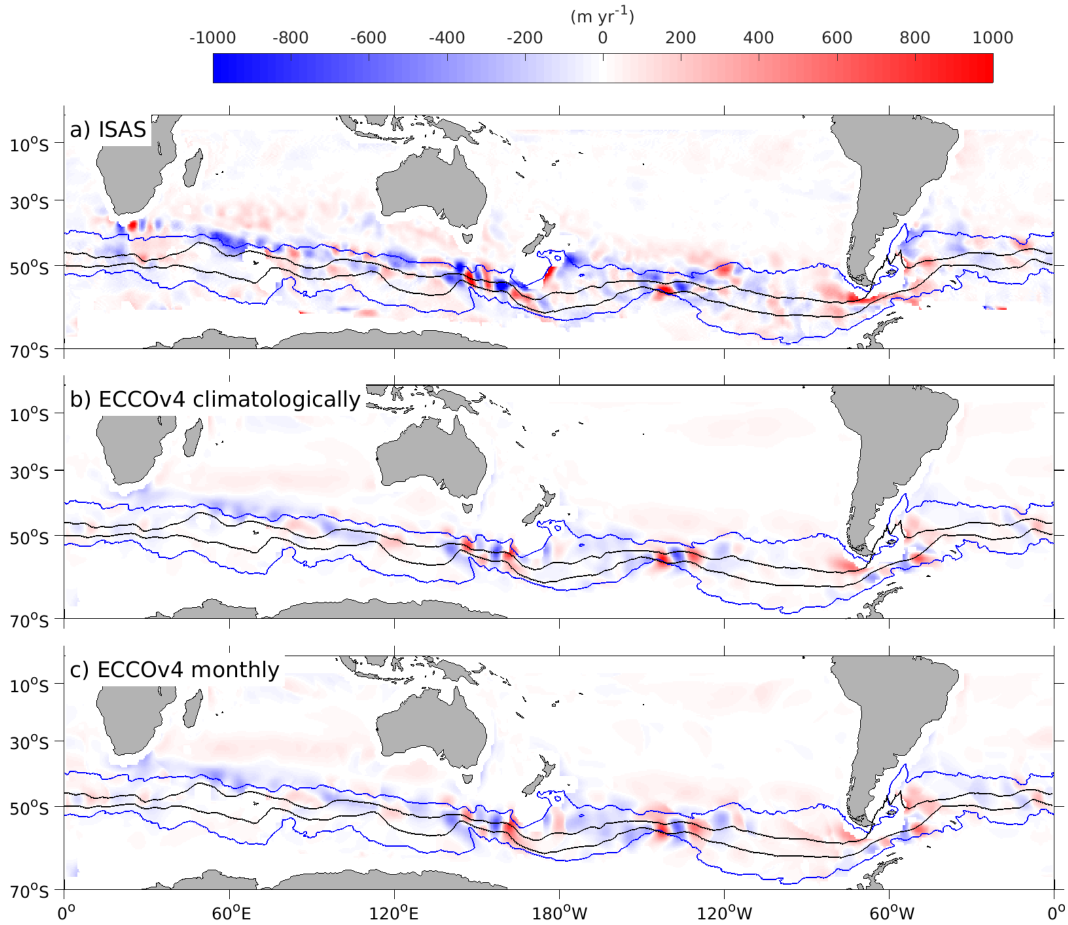

Figure S3: Lateral induction term of subduction as computed with a) ISAS by averaging the climatological induction, b) ECCOv4 in the same way as in panel a and c) ECCOv4 by time-averaging the computed monthly induction over the 10-years period between 2006 and 2015

Figure S4:

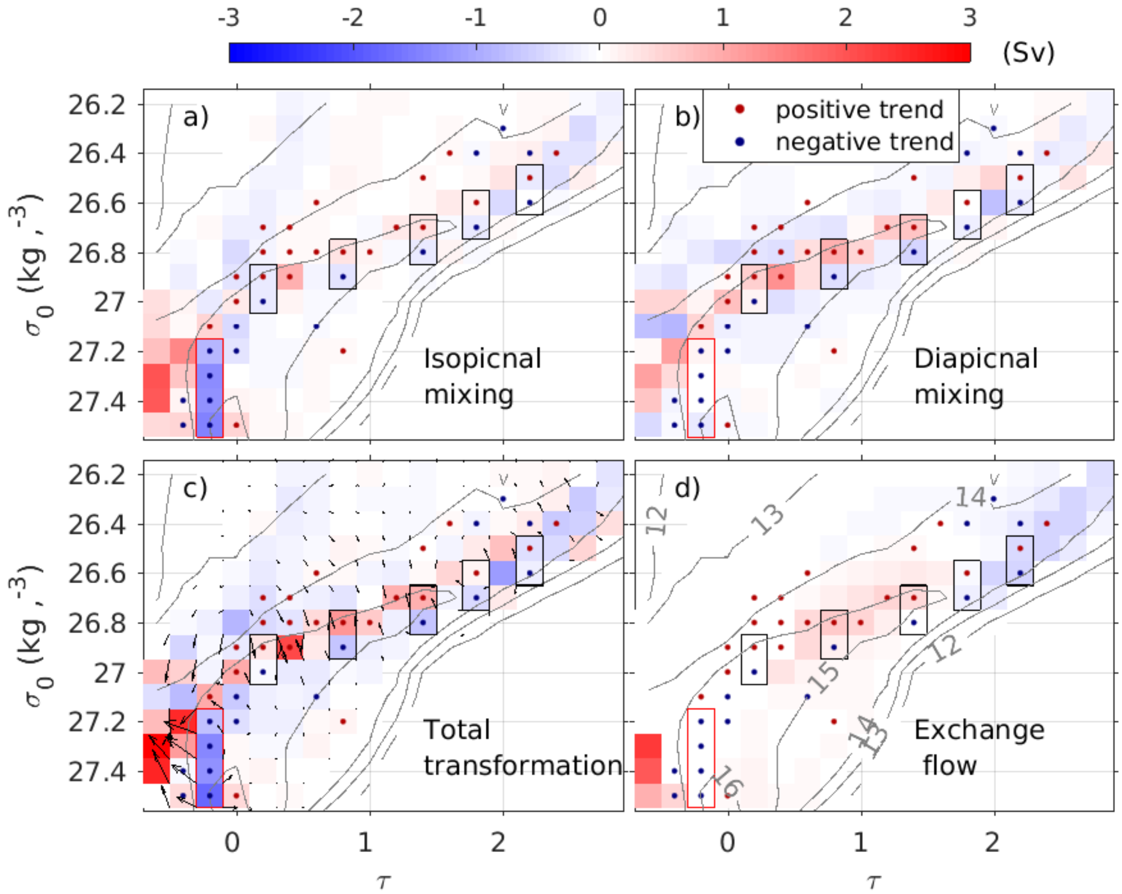

Figure S4. a) Isopicnal, b) diapycnal transformation (arrows) and formation (color coded) and c) the sum of both components. d) Exchange flow across the domain's limits where red indicates water into the domain and blue means flow out from the domain. The diagrams are shown in σ-τ coordinates.